nature publishing group

Review

Magnetic resonance imaging based noninvasive measurements of brain hemodynamics in neonates: a review

Jill B. De Vis[1], Thomas Alderliesten[2], Jeroen Hendrikse[1], Esben T. Petersen[2,3] and Manon J.N.L. Benders[1]

Perinatal disturbances of brain hemodynamics can have a detrimental effect on the brain's parenchyma with consequently adverse neurodevelopmental outcome. Noninvasive, reliable tools to evaluate the neonate's brain hemodynamics are scarce. Advances in magnetic resonance imaging have provided new methods to noninvasively assess brain hemodynamics. More recently these methods have made their transition to the neonatal population. The aim of this review is twofold. Firstly, to describe these newly available noninvasive methods to investigate brain hemodynamics in neonates. Secondly, to discuss the results that were obtained with these techniques, identifying both potential clinical applications as well as gaps of knowledge.

The developing brain is most vulnerable during the last 3 mo of fetal life and at term age when neuronal proliferation, neuronal migration, white matter myelinisation, glial cell migration, and cortical folding are at their maximum ages (1–3). Any disturbance around birth in the delivery of blood or oxygen to the brain tissue can have a deleterious effect leading to hypoxic-ischemic encephalopathy (HIE) (4,5), perinatal arterial ischemic stroke (PAIS) (6) mainly in term infants, and periventricular leukomalacia (7) especially in preterm infants, or other brain injuries, which are known to be related to adverse neurodevelopmental outcome (8–10). Therefore, a sensitive assessment of the perfusion and oxygenation status of the brain tissue is important to monitor the neonate's brain. As well, it could provide invaluable insight into the effect of neuroprotective agents. Unfortunately, the gold-standards to evaluate brain hemodynamics, oxygen-15 positron emission tomography (PET) and Xenon clearance, are invasive and therefore not feasible in neonates on a routine basis (11,12). Although, noninvasive techniques like Doppler flow measurements (13) and near-infrared spectroscopy (NIRS) (14) have been used as alternatives, these techniques have their own limitations. Given current commercial device and sensor combinations, NIRS only provides localized information (i.e., depending on sensor position) and samples at an average depth of 2 cm (15). Limitations of the Doppler technique in assessing flow are it's angle dependency and, particularly in the (preterm) neonatal population, small vessel size limits the method to the assessment of indices of flow rather than actual flow. In addition, it does not actually measure tissue perfusion (e.g., in ml/100g/min).

Advances in Magnetic Resonance Imaging (MRI) have brought forward techniques which allow noninvasive evaluation of brain hemodynamics. More recently, these techniques have made their transition to the neonatal population. This review provides an overview of cerebral hemodynamics and how they are measured by noninvasive techniques, summarizes potential clinical applications, and ends with suggestions for future research.

CEREBRAL HEMODYNAMICS

The delivery of oxygen and other nutrients to the brain tissue is essential for the brain tissue to survive. The delivery and consumption of oxygen and nutrients can be defined by four different hemodynamics parameters: the cerebral blood flow (CBF), the oxygen extraction fraction (OEF), the oxygen saturation (SO_2), and the cerebral metabolic rate of oxygen ($CMRO_2$). The different MRI techniques to measure CBF, OEF, SO_2, and $CMRO_2$ will be discussed separately.

Cerebral Blood Flow

Phase-contrast magnetic resonance angiography (PC-MRA) and arterial spin labeling (ASL) are the two noninvasive MRI-techniques available to estimate CBF. The advantage of PC-MRA as compared with ASL is the velocity with whom the images can be acquired. The disadvantage is its lack of spatial information and the post processing time required to segment conventional brain images in order to obtain a perfusion value in ml/100 g/min. Arterial spin labeling, on the other hand, does provide perfusion measurements at the brain tissue level which can be obtained with limited post processing. However, ASL is limited in signal-to-noise ratio (SNR).

In PC-MRA two flow-sensitive datasets are acquired with opposite flow-encoding gradients. The flowing protons, or spins, in the blood thereby yield a net phase shift in between the acquisition of both datasets while stationary spins (e.g., tissue)

[1]Department of Radiology, University Medical Center Utrecht, Utrecht, The Netherlands; [2]Department of Neonatology, Wilhelmina's Children's hospital/University Medical Center Utrecht, Utrecht, The Netherlands; [3]Danish Research Center for MR, Hidovre Hospital, Copenhagen, Denmark. Correspondence: Jill Britt De Vis (j.devis-2@umcutrecht)

Received 23 March 2016; accepted 15 May 2016; advance online publication 21 September 2016. doi:10.1038/pr.2016.146

do not gain a net phase shift. The magnitude of this phase shift is directly proportional to the velocity of the spins and can be expressed in cm/s. Multiplication of a vessel's cross-sectional surface area ($\pi \cdot r^2$) by the average blood velocity (in cm/s) in the same vessel, yields the actual quantity of blood (in ml/min) being transported by that vessel. Subsequently, blood flow toward the brain can be obtained by adding up the blood flow in the main feeding arteries: both internal carotid arteries and either both vertebral arteries or the basilar artery. The final step is calculating CBF (in ml/100 ml/min) by dividing total blood flow by total brain volume derived from segmentation of anatomical MR images. Division by brain density (i.e., 1.06 g/ml in neonates) (16) provides brain perfusion in more commonly reported units of ml/100 g/min. Blood flow can be measured with PC-MRA in less than a minute, in order to obtain brain perfusion one should take another few minutes for anatomical MR images into account.

The second technique, ASL is a subtraction technique where a perfusion weighted image is obtained by subtraction of a control image and a labeled image. In the labeled image, the blood signal has been inverted during the preparation phase. This is done by applying radiofrequency pulses in the neck region. The acquisition of the actual image starts at a certain delay after labeling (i.e., postlabel delay), which allows the inverted spins to reach the brain tissue through the vasculature. The difference in signal between the control and labeled images is proportional to the CBF. Each control-label pair yields a signal difference of only 1–2%, therefore, multiple control-label sets (i.e., dynamics) are acquired to increase the SNR. By averaging the signal of multiple dynamics the SNR is increased as the noise goes down with the square root of the number of dynamics. However, one needs to keep in mind that this works at the expense of a longer imaging time. The signal difference of the subtracted image can be quantified using a general kinetic model which accounts for the size of the labeled bolus, the decay of the label, the efficiency of the labeling, and the proton exchange rate between blood and tissue (17). The proton exchange rate can be considered a single constant. However, the size and decay of the label depend on the acquisition (e.g., label duration and postlabel delay), patient characteristics (i.e., the longitudinal relaxation rate or spin-lattice relaxation time of blood (T_{1b}) which depends on age and hematocrit (hct)), and the flow velocity of blood in the neck which affects label efficiency. Two research groups have measured the T_{1b} in neonates and found it to be higher and more variable in neonates compared with adults; mean 1.8 s range with reported rages of 1.4–2 s and 1.4-2.3s respectively (18,19). For comparison, adults have a typical T_{1b} of ~1.6 s (20). These variations in neonatal T_{1b} arise from the more variable hematocrit observed in infancy. More importantly, assuming an incorrect T_{1b} can introduce perfusion errors ranging from −17 to 30% (19). In addition, the label efficiency is more likely to vary in neonates and also depends on which labeling technique is being used. In general, two ASL techniques are used in neonates; pulsed ASL (PASL) and pseudocontinuous ASL (pCASL). With both techniques perfusion images can be acquired in ~3 min. In PASL a thick slab (10 cm) of arterial hydrogen protons is inverted proximal to the imaging plane at a single time point using a short radiofrequency pulse (5–20 ms), **Figure 1a**. In pCASL a train of discrete radiofrequency pulses is applied for a certain (label) duration (e.g., 1–2 s) to label the protons in the neck region just proximal to the brain, **Figure 1b** (21). Although pCASL has a higher SNR compared with PASL, its inversion efficiency is dependent on the blood's velocity (22), which is known to be quite variable in neonates (23). A comparative study between PASL and pCASL in neonates demonstrated a strong correlation between the CBF values, but, the image quality score of pCASL images was higher than PASL images (24). **Figure 1c** shows example perfusion images obtained with PASL and pCASL. The following models are used to quantify (in ml/100 g/min) PASL and pCASL images, respectively;

$$\mathrm{CBF} = \frac{6000 \cdot \lambda \left(\mathrm{SI}_{\mathrm{control}} - \mathrm{SI}_{\mathrm{label}} \right) \cdot e^{T_{1_{/T_b}}}}{2\alpha \cdot TI_1 \cdot SI_{PD}}$$

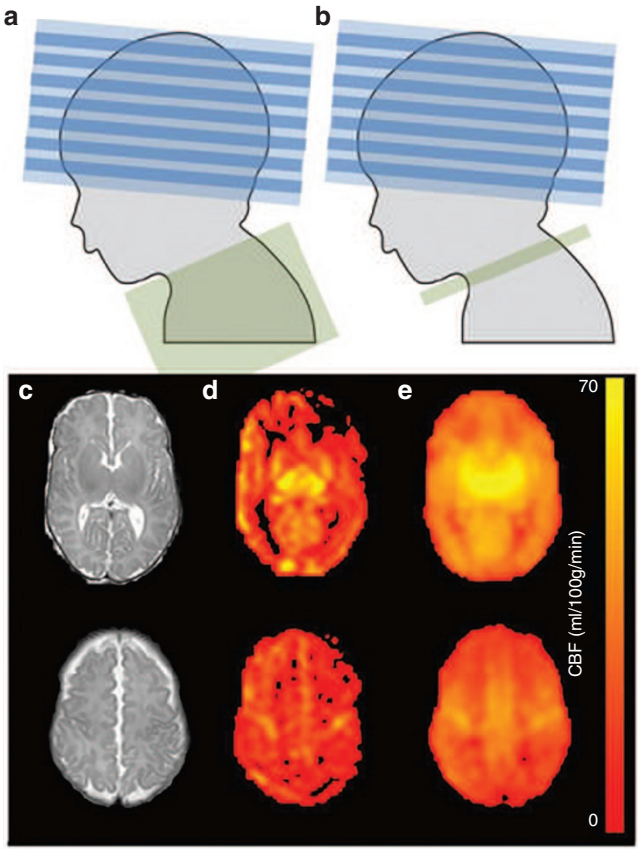

Figure 1. Pulsed and pseudocontinuous ASL. (**a**) Labeling and imaging planes of PASL; the labeling slab of PASL is around 10 cm and covers the neck region. (**b**) Labeling and imaging planes of pCASL; the labeling plane of pCASL is a thin slab just proximal of the brain on which a train of radiofrequency pulses is applied to label a pile of blood. (**c**) T_2-weighted images. (**d**) Perfusion-weighted images obtained with PASL. (**e**) Perfusion-weighted images obtained with pCASL. The images in **c**, **d**, and **e** are of the same infant. ASL, arterial spin labeling; PASL, pulsed ASL; pCASL, pseudocontinuous ASL.

$$\mathrm{CBF} = \frac{6000 \cdot \lambda \left(\mathrm{SI}_{\mathrm{control}} - \mathrm{SI}_{\mathrm{label}}\right) \cdot e^{PLD/T_b}}{2\alpha \cdot T_{1b} \cdot SI_{PD} \cdot \left(1 - e^{-\tau/T_{1b}}\right)}$$

With λ being the blood-brain partition coefficient, SI-the signal intensity, α-the inversion time, and TI-the inversion time. From the authors' experience, a postlabel delay of 1.5–2.0 s gives reliable perfusion images. In terms of the T_{1b} we would recommend to estimate its value based on hematocrit or adopt a value of 1.8 s (18,19). The λ can be set at 1.1 ml/g based on previous literature (25). No work has been published on the inversion efficiency in neonatal ASL imaging yet, we recommend 95% for PASL imaging and a conservative 85% for pCASL imaging based on its dependency of blood velocity.

Apart from these two noninvasive MRI techniques to measure CBF, the CBF can also be measured at the tissue level with the use of gadolinium-based contrast agents which causes magnetic susceptibility effects and thereby a signal drop when the contrast bolus passes through the tissue. Despite the technique being invasive as it requires the administration of a contrast agent, the contrast agents have also been related to nephrogenic systemic fibrosis in patients with renal impairment (26). This is in particular of importance in neonates due to their immature renal function. The advantage of gadolinium-based perfusion-weighted imaging over ASL is the fact that the contrast bolus induces larger signal changes as compared with the labeled spins in ASL imaging. The reliability of perfusion images is further increased in children due to their higher heart rate and faster circulation times which narrow the contrast bolus (27).

The SO_2 and the OEF

The techniques to measure the cerebral SO_2 in neonates can be roughly divided into two groups (1); the susceptometry-based measurements (28) and (2) the T_2-based measurements (29–33). The T_2-based measurements rely on the transverse (or spin-spin) relaxation time of blood (T_{2b}) and are T_2-relaxation-under-spin-tagging (29–31), T_2-prepared tissue relaxation with inversion recovery (T_2-TRIR) (32) and T_2-prepared blood imaging of oxygen saturation (T_2-BIOS) (33). The OEF is the difference between the arterial oxygen saturation-S_aO_2, obtained by pulse oximetry, and the venous oxygen saturation-S_vO_2, obtained in the sagittal sinus.

Susceptometry-based measurements, rely on the relative magnetic susceptibility difference between intravascular blood and surrounding tissue (34). As deoxygenated hemoglobin is paramagnetic, the extent to which the local magnetic field is disturbed depends on the blood oxygenation level. Intravascular protons sense a slightly larger magnetic field, which results in a susceptibility difference between intravascular and extravascular protons. The shifts in magnetic field can be quantified by measuring the phases of the MRI signal, and thereby the oxygenation level of blood can be quantified. In more or less a minute time the S_vO_2 can be measured in the sagittal sinus using SBM.

In the T_2-based measurements the transverse relaxation rate of pure blood (T_{2b}) is measured. The T_2 has a known relation with oxygenation (Y) and Hct, therefore the T_{2b} can be converted into SO_2 by means of a calibration plot obtained through *in vitro* measurements on adult and neonatal blood (29,35). The difference in T_2-relaxation-under-spin-tagging (~80 s, T_2-TRIR (~90 s) and T_2-BIOS (~270 s) lies in the approach used to isolate the signal coming from blood. Both T_2-relaxation-under-spin-tagging and T_2-TRIR target the sagittal sinus and thus obtain venous T_{2b}, and thus Y_v. Consequently, from Y_v the OEF can be calculated when the arterial oxygenation (Y_a) is known.

$$\mathrm{OEF} = \frac{\left(Y_a - Y_v\right)}{Y_a} 100$$

In T_2-relaxation-under-spin-tagging the blood is magnetically labeled and isolated using a similar principle of control minus label image as is used in ASL MRI. Hereby contamination by signal from surrounding tissue and cerebrospinal fluid is avoided (30). Instead, the T_2-TRIR uses an image saturation module to suppress signal from tissue types other than blood. The inflowing blood has not been suppressed previously and will be the only source of signal (**Figure 2**). The T_2-BIOS technique (33) on the other hand isolates the blood signal by exploiting Intravoxel incoherent motion imaging (36,37). This way blood in arterial, capillary, and venous vessels is targeted and an overall T_{2b} of a mixed

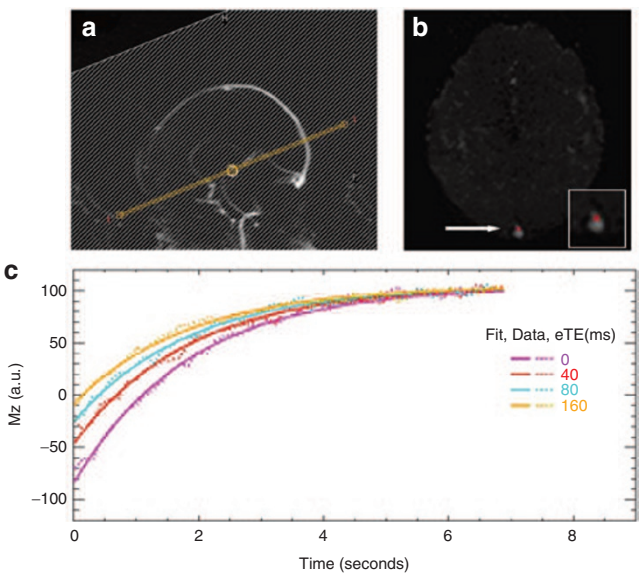

Figure 2. The T_2-TRIR sequence. (**a**) The image shows the planning of the T_2-TRIR sequence. The T_2-TRIR sequence incorporates a whole-brain T_2 preparation scheme (white stripes) while the imaging plane (yellow) receives a presaturation pulse. This way the signal from all tissue within the imaging plane is suppressed and only T_2-prepared inflowing blood in the sagittal sinus is depicted (see panel **b**). An automatic region-of-interest is than chosen within the sagittal sinus and from the signal intensities within this area the T_2 of blood can be obtained (see panel **c**).

Table 1. Multimodality studies

Study	Modality 1	Modality 2	Population	Values
CBF				
Benders *et al.*, 2013 (38)	wCBF (PC-MRA)	wCBF (Doppler)	Various	$r = 0.51, P < 0.01$
Wintermark *et al.*, 2014 (40)	wCBF (ASL)	SO_2 (NIRS)	Severe HIE	$R^2 = 0.77, P < 0.01$
	wCBF (ASL)	SO_2 (NIRS)	Moderate HIE	$R^2 = 0.14, P = 0.74$
Alderliesten *et al.*, 2012 (33)	wCBF (ASL)	SO_2 (NIRS)	Various	$R^2 = 0.50, P < 0.01$
	fCBF ASL)	SO_2 (NIRS)	Various	$R^2 = 0.71, P < 0.001$
Jain *et al.*, 2014 (39)	wCBF (ASL)	SO_2 (NIRS)	CHD	$R^2 = 0.67$, P < 0.001
Massaro *et al.* 2013 (41)	wCBF	SO_2 (NIRS)	HIE 2nd week	ns
SO_2				
Alderliesten *et al.*, 2012 (33)	*Yv* (T_2-TRIR)	SO_2 (NIRS)	Various	$R^2 = 0.65, P < 0.01$
	SO_2 (T_2-BIOS)	SO_2 (NIRS)		$R^2 = 0.64, P < 0.001$
	SO_2 (T_2-BIOS)	*Yv* (T_2-TRIR)		$R^2 = 0.49, P < 0.05$
Jain *et al.*, 2014 (39)	*Yv* (SBM)	SO_2 (NIRS)	CHD	$R^2 = 0.69, P < 0.001$
$CMRO_2$				
Jain *et al.*, 2014 (39)	$CMRO_2$	SO_2 (NIRS)	CHD	$R^2 = 0.67, P < 0.001$

Overview of the studies which have compared the magnetic resonance imaging (MRI)-hemodynamic measurements to non-MRI hemodynamic evaluation tools.
ASL, arterial spin labeling; CBF, cerebral blood flow; CHD, congenital heart disease; $CMRO_2$, cerebral metabolic rate of oxygen; fCBF, frontal CBF; HIE, hypoxic-ischemic encephalopathy; NIRS, near-infrared spectroscopy; ns, non-significant; PC-MRA, phase-contrast magnetic resonance angiography; SBM, susceptometry-based measurements; SO_2, oxygen saturation; T_2-BIOS, T_2-prepared blood imaging of oxygen saturation; T_2-TRIR, T_2-prepared tissue relaxation with inversion recovery; wCBF, whole brain CBF.

vascular compartment is obtained. In theory, this mixed compartment is comparable to the compartment that is being measured by NIRS. The advantage of the T_2-BIOS over NIRS is that it also provides a SO_2 estimate of the deeper gray and white matter.

The $CMRO_2$ (in μmol/100 g/min) is the actual tissue consumption of oxygen and can be defined as the OEF times the CBF, while accounting for the oxygen carrying capacity of blood (i.e., Hb-bound O_2 and O_2 dissolved in plasma; C_a) (31,32).

$$\mathrm{CMRO_2} = \mathrm{CBF}\left(Y_a - Y_v\right)C_a$$

MULTIMODALITY STUDIES

Several studies have demonstrated associations between hemodynamic parameters assessed by different modalities (**Table 1**). This cross-validates the different techniques and strengthens confidence in their use a measure of cerebral hemodynamics.

CBF measured by PC-MRA correlated positively with CBF values obtained by Doppler ultrasound. Nevertheless, limits-of-agreement were wide (−78 to +68), most markedly at higher CBF (38). NIRS-SO_2 has been found to have a strong correlation with both whole brain and frontal CBF (33,39,40). Interestingly, the group of Massaro *et al.* did not find a strong relation between NIRS-SO_2 and CBF during the second week after HIE (41). However, in this study, spot NIRS measurements instead of continuous NIRS tracings were analyzed and the measurements were not necessarily obtained in close proximity to MR imaging.

A good relation was found between NIRS-SO_2 and MRI-SO_2/Y_v measured by either T_2-TRIR, T_2-BIOS or susceptometry-based measurements (33,39). A cross-validation of the T_2-TRIR and T_2-BIOS technique found a moderate relation (33). Overall, we could say that the different measurements relate to each other, which brings support for their further evaluation in clinical research studies.

CLINICAL APPLICATIONS

Thus far, the main focus in terms of clinical applications has been on brain maturation in preterm infants, infants with PAIS, with HIE, and infants with congenital heart disease (CHD). The results of these studies are summarized in **Table 2**.

Brain Maturation

Two studies evaluated CBF using PC-MRA and both of them found an increase in CBF with postconceptional age (42,43). In the study of Benders *et al.*, the CBF ranged from 11 to 48 ml/min/kg body weight in infants ranging from 30 to 51 wk postconceptional age (42). Varela *et al.* found CBF to vary from 24–56 ml/100 g/min brain tissue in infants with a postconceptional of 30–95 wk (43). Moreover, in this last study, a steep rise in CBF was noticed in between 47 and 62 wk of postconceptional age (38). A study performed using ASL (44) found a similar increase in CBF with age; from 7 –29 ml/100 g/min in infants ranging from 29 –50 wk postconceptional age. In their study, CBF was highest in the deep gray matter. Similarly, Miranda *et al.* found a significant higher perfusion in the basal ganglia than in the cortical gray matter of term neonates and preterm neonates at term-equivalent age and it was hypothesized that these regional differences were caused by developmental

Table 2. MRI measurements of hemodynamic parameters

Study	Method	Parameter	Age	*N*	Values
Brain maturation					
Benders *et al.*, 2011 (42)	PC-MRA	CBF	30–51 w PCA	30	25 (range: 11-48) ml/min/kg body weight
Varela *et al.*, 2012 (43)	PC-MRA	CBF	30–95 w PCA	21	range: 18-60 ml/100g/min
De Vis *et al.*, 2013 (44)	ASL	CBF	29–50 w PCA	29	range: 7-29 ml/100g/min
Miranda *et al.*, 2006 (45)	ASL	CBF	PT-TEA	23	21.3 ± 5.1 ml/100g/min
Liu *et al.*, 2014 (52)	PC-MRA; TRUST	CBF; Y_v	33–40 w PCA	12	13.4 ± 4.2; 62.6 ± 8.3%
De Vis *et al.*, 2014 (32)	T_2-TRIR	Y_v	26–48 w PCA	42	59 ± 14%
Liu *et al.*, 2014 (52)	TRUST/PC-MRA	$CMRO_2$	33–40 w PCA	12	38.3 ± 17.7 μmol/100g/min
De Vis *et al.*, 2014 (32)	T_2-TRIR/ASL	$CMRO_2$	26–48 w PCA	22	30 ± 12 μmol/100g/min
PAIS					
Van der Aa *et al.*, 2012 (54)	PC-MRA	Flow	w 1/3 mo	17	Asymmetry (ipsilateral/contralateral): 8.5%/1.0%
De Vis *et al.*, 2013 (56)	PC-MRA	Flow	w 1	4	Asymmetry (ipsilateral/contralateral): 9.5%
De Vis *et al.*, 2013 (56)	ASL	CBF	w 1	4	Ipsilateral/contralateral: 11.5 ± 3.3 / 12.2 ± 2.1 ml/100g/min
HIE					
De Vis *et al.*, 2015 (60)	ASL	CBF	HIE adverse outcome bgt HIE good outcome bgt	20; 8	63 (28–108) ml/100g/min; 28 (12–51) ml/100g/min
Shi *et al.*, 2012 (61)	ASL	CBF	HIE gm/wm/bg; Controls gm/wm/bg	33; 7	153 ± 12 / 71 ± 10 / 217 ± 13 SI; 125 ± 12/ 73 ± 12 / 174 ± 15 SI
Massaro *et al.*,2013 (41)	ASL	CBF	HIE wb/bg/wm; Controls wb/bg/wm	18; 18	24 ± 5 / 52 ± 19 / 12 ± 3 ml/100g/min; 19 ± 2 /31 ± 5/10 ± 2 ml/100g/min
De Vis *et al.*, 2014 (32)	ASL	CBF	HIE; Controls	9; 10	12 ± 4 ml/100g/min; 14 ± 3 ml/100g/min
	T_2-TRIR	Y_v	HIE; Controls	11; 17	66 ± 12%; 50 ± 11%
	T_2-TRIR/ASL	$CMRO_2$	HIE; Controls	9; 10	24 ± 12 μmol/100g/min; 30 ± 6 μmol/100g/min
CHD					
Licht *et al.*, 2004 (67)	ASL	CBF; CBF HC	CHD	25	19.7 ± 9.2 ml/100g/min; 40.1 ± 20.3 ml/100g/min
Jain *et al.*, 2014 (39)	SBM	Y_v Yv HC	CHD	32	55.2 (IQR: 49.3, 60.2)%; 66.4 (IQR: 57.0,72.5)%
	ASL	CBF CBF HC			9.6 (IQR: 7.5,15.1) ml/100g/min; 21.2 (IQR: 16.5,31.0) ml/100g/min
	SBM+ASL	$CMRO_2$; $CMRO_2$ HC			0.49 (IGR: 0.4, 0.79) ml O_2/100g/min; 0.53 (IQR: 0.4. 0.79) ml O2/100g/min
Nagaraj *et al.*, 2015 (68).	ASL	CBF	CHD; Controls	43; 58	16.3 ml/100g/min; 19.3 ml/100g/min

ASL, arterial spin labeling; bg, basal ganglia; bgt, basal ganglia and thalami; CBF, cerebral blood flow; CHD, congenital heart disease; $CMRO_2$, cerebral metabolic rate of oxygen; gm, gray matter; HC, hypercapnia; HIE, hypoxic-ischemic encephalopathy; MRI, magnetic resonance imaging; PAIS, perinatal arterial ischemic stroke; PCA, postconceptional age; PC-MRA, phase-contrast magnetic resonance angiography; PT-TEA, preterm at term-equivalent age; SBM, Susceptometry-based measurements; SI, signal intensity; T_2-TRIR, T_2-prepared tissue relaxation with inversion recovery; wb, whole brain; wm, white matter.
This table gives an overview of the results of the different studies which have measured the brain hemodynamic parameters with noninvasive MRI techniques. The results are grouped in; brain maturation, PAIS, HIE, and CHD. The results are either presented as mean ± SD, median (range) or mean (interquartile range, IQR).

processes (45). The increase in CBF with postconceptional age reflects brain maturation and is consistent with previously performed positron emission tomography and xenon-enhanced computed tomography studies (Xe-CT) (46–51). For an overview of these earlier found values, see **Table 3**. **Figure 3** shows ASL images of a preterm infant imaged at preterm age and at term-equivalent age, the increase in perfusion with gestational age can be appreciated on these images. As well, it can be noted that the perfusion is higher in the occipital than in the frontal cortex. This is related to brain development and is similar to the results found in diffusion-tensor imaging studies and studies on cortical folding.

T_2-based measurements of venous oxygenation (Y_v) found mean values of 64 and 59% in infants with a postconceptional age of 33–40 wk and 26–48 wk respectively (32,52). The mean $CMRO_2$ values found in these studies were 38 and 30 μmol/100 g/min. Interestingly, both studies found an increase in the $CMRO_2$ with both postconceptional and postnatal age. Similar to the CBF measurements, the $CMRO_2$ measurements obtained by the newly developed noninvasive MRI techniques

Table 3. Non-MRI measurements of hemodynamic parameters

Study	Method	Age	Category	*N*	Values
CBF (in ml/100g/min)					
Chiron *et al.*, 1992 (46)	Xe-CT	2–45 d PNA; 2–7 m PNA	Healthy; Healthy	7; 7	50 ± 3.4; 55 ± 5.3
Pryds *et al.*, 1989 (47)	Xe-CT	<35 w	RDS	22	8.4-11.5 (3.6–28.9)
Skov *et al.*, 1993 (48)	NIRS	24–37 PCA	RDS; HIE	22; 10	12.6 ± 6.4; 26.5 ± 17.9
Altman *et al.*, 1993 (49)	PET	24–39 PCA	HIE, others	11	21.6 ± 21
Yoxall *et al.*, 1998 (50)	NIRS	22–39 PCA	Seizures, others	20	9.3 (4.5 – 28.3)
Tyszuk *et al.*, 1998 (51)	NIRS	24–34	Preterm	30	13.9 ± 6.9/12.3 ± 6.4
Y_v *(in %)*					
Skov *et al.*, 1993 (48)	NIRS	24–37 PCA	RDS, HIE	22; 10	53.44 ± 15.36; 67.3 ± 9.38
Yoxall *et al.*, 1998 (50)	NIRS	22–39 PCA	Seizures, others	20	64.6 (76.1 – 46.8)
Zaramella *et al.*, 2007 (53)	NIRS		HIE; Controls	22; 15	75.3 (54.8 – 99); 66.4 (55.9 – 88.8)
$CMRO_2$ *(in µmol/100g/min)*					
Skov *et al.*,1993 (48)	NIRS	24–37 PCA	RDS; HIE	22; 10	44.7 ± 17.9; 62.6 ± 35.8
Altman *et al.*,1993 (49)	PET	24–39 PCA	HIE, others	11	21.4 ± 16.4
Yoxall *et al.*,1998 (50)	NIRS	22–39 PCA	Seizures, others	20	23.1 (8.6 –78.5)

CBF, cerebral blood flow; $CMRO_2$, cerebral metabolic rate of oxygen; gm, gray matter; HIE, hypoxic-ischemic encephalopathy; MRI, magnetic resonance imaging; NIRS, near-infrared spectroscopy; PCA, postconceptional age; PET, positron emission tomography; PNA, postnatal age; RDS, respiratory distress syndrome; Xe-CT, xenon-enhanced computed tomography studies; T_2-based measurements of venous oxygenation.
This table gives an overview of the studies which have assessed the brain hemodynamic parameters with techniques other than MRI. The results of these studies are grouped per hemodynamic parameter; CBF, Y_v and $CMRO_2$.

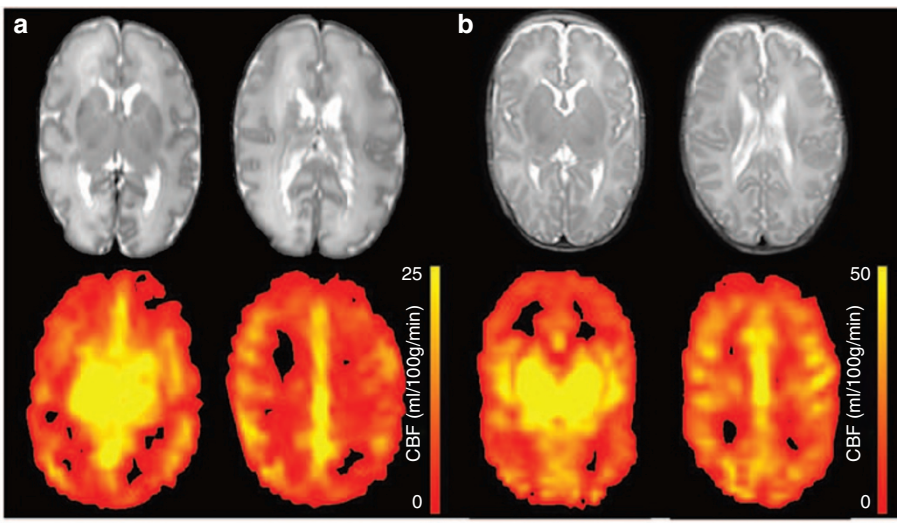

Figure 3. Brain maturation. Images of an infant born at preterm age (30 wk postconceptional age). (**a**) T_2-weighted images and PASL images obtained at 31 wk postconceptional age, the brain perfusion is shown in ml/100g/min (see color bar). (**b**) T_2-weighted images and PASL images obtained at a postconceptional age of 38 wk. Note that the color bar has a higher scale than in **a**, this was necessary because the perfusion was increased as compared with the images obtained at preterm age. ASL, arterial spin labeling; PASL, pulsed ASL.

are in a similar order of magnitude as the values found earlier in positron emission tomography and NIRS studies (Table 3) (48–50,53).

Perinatal Arterial Ischemic Stroke

A study performed using PC-MRA demonstrated a higher blood flow in the ipsilateral ICA during the acute phase after unilateral PAIS. This increased blood flow toward the affected side disappeared after 3 mo and no relation was found between this asymmetry in blood flow and stroke size (54). When using ASL, an increased CBF was found in one out of four patients. The remaining three patients demonstrated a decreased CBF in the stroke center, however with increased CBF in the periphery of the stroke region (55). Similar perfusion patterns were described in a second ASL MRI study (56). In this study, one patient presented with hyperperfusion, whereas the remaining three presented with hypoperfusion and only one of them had hyperperfusion in the periphery of the stroke area. As

compared with the PC-MRA study, perfusion at follow-up was comparable between the affected and unaffected side. It can be concluded that hyperperfusion can occur at certain time intervals after stroke in neonates. Depending of the location of this phenomenon, it could be comparable to "luxury perfusion" described in adult stroke. It has been suggested that the luxury perfusion represents physiologic transient reperfusion via recanalization and/or collateral flow, which might be a marker for tissue survival and protective for hemorrhagic transformation (57–59). **Figure 4**, panel a shows ASL images of an infant with PAIS.

Hypoxic-ischemic Encephalopathy

Two studies found a higher perfusion in the deep gray matter of the infants with HIE and poor outcome; De Vis *et al.* reported 63 vs. 28 ml/100 g/min with a 85% sensitivity and 100% specificity for adverse outcome at a cut-off of 51 ml/100 g/min (60). Shi *et al.* did not quantify perfusion, but found significant higher signal intensity in the gray matter and basal ganglia of infants with HIE (61). Pienaar *et al.* found a negative correlation between the apparent-diffusion-coefficient and CBF in nine neonates with clinical and imaging evidence of ischemia, which suggests that cerebral tissue damage is associated with hyperperfusion (62). A single study described the evolution of perfusion during the first week after the hypoxic-ischemic event. Initial hypoperfusion on day 1 was followed by hyperperfusion in brain areas that subsequently exhibited brain injury on conventional images (63). Another study evaluated the brain tissue perfusion in the second week after the hypoxic-ischemic event and found global and regional CBF to be still higher in infants with HIE (64). Among the infants with HIE, infants with injury on MR imaging had a lower CBF in the thalamus. This was attributed to pseudonormalization of CBF and low metabolic demand after progression to irreversible brain injury (41). **Figure 4b** shows ASL images of an infant with HIE.

Thus far, only one paper described MRI-based measurements of venous oxygenation (Y_v) and $CMRO_2$ in infants with HIE (32). In this study, the Y_v in infants with HIE was found to be higher than in controls (66% vs. 50%), suggesting lower oxygen consumption caused by tissue injury. No significant differences in CBF and $CMRO_2$ were found, possibly due to the smaller sample size. Derangements in oxygen consumption in neonates with HIE, measured by magnetic resonance spectroscopy, have been found to be related to adverse neurodevelopmental outcome (65).

Congenital Heart Disease

Neonates with CHD can be a particular difficult group in which to perform ASL perfusion measurements. This is because vascular shunts between the pulmonary and arterial circulation can decrease the body circulation time of labeled blood. Goff *et al.* demonstrated that the amount of negative voxels in neonates with CHD increases when the CBF is decreased, thus potentially introducing errors in the CBF measurements (66). A way to decrease the number of negative perfusion voxels is by restricting the labeling volume (67). In infants with CHD a decreased CBF and a smaller change in CBF under hypercarbia circumstances was shown to relate to periventricular leukomalacia (68). Nagaraj *et al.* found lower global and regional (basal ganglia) CBF in infants with CHD compared with controls. Within the group of infants with CHD, infants with cyanotic CHD had lower CBF in the basal ganglia, thalami, and occipital white matter compared with infants with acyanotic CHD (69). Susceptometry-based $CMRO_2$ measurements were performed in neonates with CHD but have thus far not been compared with measurements in control neonates (39).

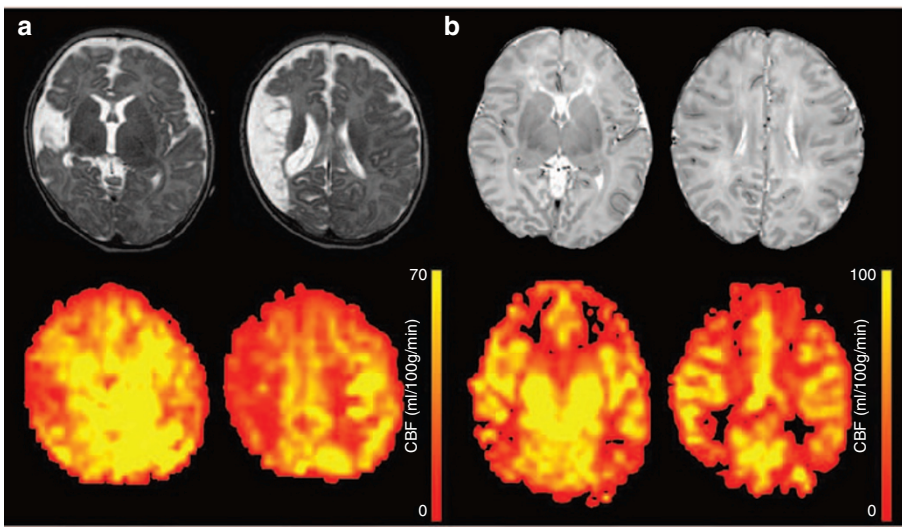

Figure 4. Perinatal arterial ischemic stroke and hypoxic-ischemic encephalopathy. (**a**) T_2-weighted images and PASL images of an infant with PAIS in the territory of the right middle cerebral artery (MCA). On the T_2-weighted images tissue loss is seen within the right MCA area. Within this same area, a lower perfusion is seen on the PASL (images. **b**) T_2-weighted images and PASL images of an infant with HIE. The brain tissue of this infant demonstrated a profound hyperperfusion; this is in particular noticeable on the scale of the color bar, which had to be increased up to 100 ml/100 g/min. ASL, arterial spin labeling; HIE, hypoxic-ischemic encephalopathy; PAIS, perinatal arterial ischemic stroke; PASL, pulsed ASL.

FUTURE RESEARCH

Thus far, the reported (disease) populations are small and heterogeneous. There is a need for larger sample sizes and robust normative data in terms of postconceptional and postnatal age. In this regard, neonatal hemodynamic imaging could benefit from (inter)national collaborations in which patients with specific diseases are pooled. Multicentre studies could also help to resolve particular research questions. In PAIS, studies should be performed to investigate the relation between the different perfusion patterns (over time) and outcome. In addition, imaging of the SO_2 or OEF on a voxel-by-voxel basis with MRI sequences such as quixotic (70) (as has been proposed in adults), combined with DWI could potentially identify the penumbra and thus could predict outcome. In neonates with HIE, the course of the brain perfusion beyond the first week after the event is unclear. As well, the profit of oxygen metabolism measurements and their relation with outcome should be investigated further. Hemodynamic evaluation of infants with CHD, both before and after surgery, should be compared with hemodynamic measurements performed in healthy controls. In general, the number of clinical conditions in which hemodynamic imaging have been used is relatively limited and should be increased. Clinicians and researchers should be convinced to include these forms of imaging in their protocol, this way, larger amounts of data could be obtained making it easier to draw conclusions. From a technical point of view, we should strive for a standardized readily interpretable and accessible imaging protocol.

Efforts should be undertaken to apply sequences with minimum motion-sensitivity. In general, shorter sequences equal less motion artefacts. Furthermore, it is recommended to apply background suppression in ASL. As well, 3D-readouts, single shot imaging methods or stack-of spiral acquisitions could be used (17). Furthermore, further investigation need to be performed to assess if pCASL does indeed perform better than PASL, as this investigation was thus far only performed in neonates with HIE and in nonrandom order. Furthermore, the actual labeling efficiency in pCASL should be investigated. More specifically, for neonates with CHD an optimal imaging protocol could reduce the number of negative perfusion voxels and thereby semistandardize perfusion weighted imaging in this patient group. In this respect, it would be interesting to evaluate the performance of the different sequences. In addition, voxel-by-voxel methods, specifically for the oxygenation measurements, should be developed and improved to provide full brain coverage with sufficient SNR. Making the sequences themselves more robust would convince clinical researchers and even clinicians more to investigate the additional clinical value of those sequences and to even apply them in clinical care.

CONCLUSION

The three main noninvasive MRI techniques that are currently available to the neonatal population to image cerebral hemodynamics are PC-MRA, ASL, and T_2-based and susceptometry-based measurements of (venous) oxygenation. Thus far, ASL during the first week of life in infants with HIE is most studied and has direct evidence of clinical application. A higher CBF on day 1–7 predicts worse outcome and can be used to direct care and provide prognostic information in relation with the clinical findings. For most other conditions we can conclude that the power lies in the numbers. These hemodynamic tools clearly have some additional value, but we need to increase the numbers, standardize and optimize the research and imaging protocols to draw unequivocal conclusions that can be beneficial on an individual basis in daily clinical care.

STATEMENT OF FINANCIAL SUPPORT

No financial support was obtained for this study.

Disclosure: The authors have no conflict of interest to disclose.

REFERENCES

1. Childs AM, Ramenghi LA, Cornette L, et al. Cerebral maturation in premature infants: quantitative assessment using MR imaging. AJNR Am J Neuroradiol 2001;22:1577–82.
2. Su P, Kuan CC, Kaga K, Sano M, Mima K. Myelination progression in language-correlated regions in brain of normal children determined by quantitative MRI assessment. Int J Pediatr Otorhinolaryngol 2008;72:1751–63.
3. Provenzale JM, Liang L, DeLong D, White LE. Diffusion tensor imaging assessment of brain white matter maturation during the first postnatal year. AJR Am J Roentgenol 2007;189:476–86.
4. Himmelmann K, Hagberg G, Beckung E, Hagberg B, Uvebrant P. The changing panorama of cerebral palsy in Sweden. IX. Prevalence and origin in the birth-year period 1995-1998. Acta Paediatr 2005;94:287–94.
5. Wyatt JS, Gluckman PD, Liu PY, et al.; CoolCap Study Group. Determinants of outcomes after head cooling for neonatal encephalopathy. Pediatr 2007;119:912–21.
6. Kirton A, deVeber G. Advances in perinatal ischemic stroke. Pediatr Neurol 2009;40:205–14.
7. Khwaja O, Volpe JJ. Pathogenesis of cerebral white matter injury of prematurity. Arch Dis Child Fetal Neonatal Ed 2008;93:F153–61.
8. Kiechl-Kohlendorfer U, Ralser E, Pupp Peglow U, Reiter G, Trawöger R. Adverse neurodevelopmental outcome in preterm infants: risk factor profiles for different gestational ages. Acta Paediatr 2009;98:792–6.
9. Pape KE, Wigglesworth JS. Haemorrhage, Ischaemia, and the Perinatal Brain. London, England: Mac Keith Press, 1993:1–196.
10. Trescher WH, Lehman RA, Vannucci RC. The influence of growth retardation on perinatal hypoxic-ischemic brain damage. Early Hum Dev 1990;21:165–73.
11. Mintun MA, Raichle ME, Martin WR, Herscovitch P. Brain oxygen utilization measured with O-15 radiotracers and positron emission tomography. J Nucl Med 1984;25:177–87.
12. Skov L, Pryds O, Greisen G, Lou H. Estimation of cerebral venous saturation in newborn infants by near infrared spectroscopy. Pediatr Res 1993;33:52–5.
13. de Vries LS, van Bel F. Doppler ultrasound and periventricular leukomalacia. Pediatr 2006;117:212–3.
14. Alderliesten T, Lemmers PM, Smarius JJ, van de Vosse RE, Baerts W, van Bel F. Cerebral oxygenation, extraction, and autoregulation in very preterm infants who develop peri-intraventricular hemorrhage. J Pediatr 2013;162:698–704.e2.
15. Boas DA, Dale AM, Franceschini MA. Diffuse optical imaging of brain activation: approaches to optimizing image sensitivity, resolution, and accuracy. Neuroimage 2004;23 Suppl 1:S275–88.
16. Herscovitch P, Raichle ME. What is the correct value for the brain–blood partition coefficient for water? J Cereb Blood Flow Metab 1985;5:65–9.
17. Alsop DC, Detre JA, Golay X, et al. Recommended implementation of arterial spin-labeled perfusion MRI for clinical applications: A consensus of the ISMRM perfusion study group and the European consortium for ASL in dementia. Magn Reson Med 2015;73:102–16.

18. Varela M, Hajnal JV, Petersen ET, Golay X, Merchant N, Larkman DJ. A method for rapid *in vivo* measurement of blood T1. NMR Biomed 2011;24:80–8.
19. De Vis JB, Hendrikse J, Groenendaal F, et al. Impact of neonate haematocrit variability on the longitudinal relaxation time of blood: Implications for arterial spin labelling MRI. Neuroimage Clin 2014;4:517–25.
20. Gevers S, van Osch MJ, Bokkers RP, et al. Intra- and multicenter reproducibility of pulsed, continuous and pseudo-continuous arterial spin labeling methods for measuring cerebral perfusion. J Cereb Blood Flow Metab 2011;31:1706–15.
21. Edelman RR, Siewert B, Darby DG, et al. Qualitative mapping of cerebral blood flow and functional localization with echo-planar MR imaging and signal targeting with alternating radio frequency. Radiol 1994;192:513–20.
22. Hernandez-Garcia L, Lewis DP, Moffat B, Branch CA. Magnetization transfer effects on the efficiency of flow-driven adiabatic fast passage inversion of arterial blood. NMR Biomed 2007;20:733–42.
23. Raju TN, Go M, Ryva JC, Schmidt DJ. Common carotid artery flow velocity measurements in the newborn period with pulsed Doppler technique. Biol Neonate 1987;52:241–9.
24. Boudes E, Gilbert G, Leppert IR, et al. Measurement of brain perfusion in newborns: pulsed arterial spin labeling (PASL) versus pseudo-continuous arterial spin labeling (pCASL). Neuroimage Clin 2014;6:126–33.
25. Herscovitch P, Raichle ME. What is the correct value for the brain–blood partition coefficient for water? J Cereb Blood Flow Metab 1985;5:65–9.
26. Khawaja AZ, Cassidy DB, Al Shakarchi J, McGrogan DG, Inston NG, Jones RG. Revisiting the risks of MRI with Gadolinium based contrast agents-review of literature and guidelines. Insights Imaging 2015;6:553–8.
27. Huisman TA, Sorensen AG. Perfusion-weighted magnetic resonance imaging of the brain: techniques and application in children. Eur Radiol 2004;14:59–72.
28. Jain V, Langham MC, Floyd TF, Jain G, Magland JF, Wehrli FW. Rapid magnetic resonance measurement of global cerebral metabolic rate of oxygen consumption in humans during rest and hypercapnia. J Cereb Blood Flow Metab 2011;31:1504–12.
29. Lu H, Xu F, Grgac K, Liu P, Qin Q, van Zijl P. Calibration and validation of TRUST MRI for the estimation of cerebral blood oxygenation. Magn Reson Med 2012;67:42–9.
30. Lu H, Ge Y. Quantitative evaluation of oxygenation in venous vessels using T2-Relaxation-Under-Spin-Tagging MRI. Magn Reson Med 2008;60:357–63.
31. Xu F, Uh J, Liu P, Lu H. On improving the speed and reliability of T2-relaxation-under-spin-tagging (TRUST) MRI. Magn Reson Med 2012;68:198–204.
32. De Vis JB, Petersen ET, Alderliesten T, et al. Non-invasive MRI measurements of venous oxygenation, oxygen extraction fraction and oxygen consumption in neonates. Neuroimage 2014;95:185–92.
33. Alderliesten T, De Vis JB, Kersbergen KJ, et al. Brain oxygen saturation assessment in neonates using T2 prepared diffusion imaging and near-infrared spectroscopy. Poster presentation at the PAS 2012 International Conference, Boston, MA.
34. Jain V, Langham MC, Wehrli FW. MRI estimation of global brain oxygen consumption rate. J Cereb Blood Flow Metab 2010;30:1598–607.
35. Liu P, Chalak LF, Krishnamurthy LC, et al. T1 and T2 values of human neonatal blood at 3 Tesla: Dependence on hematocrit, oxygenation, and temperature. Magn Reson Med 2016;75:1730–5.
36. Le Bihan D, Turner R. The capillary network: a link between IVIM and classical perfusion. Magn Reson Med 1992;27:171–8.
37. Wirestam R, Brockstedt S, Lindgren A, et al. The perfusion fraction in volunteers and in patients with ischaemic stroke. Acta Radiol 1997;38:961–4.
38. Benders MJ, Hendrikse J, de Vries L, Groenendaal F, van Bel F. Doppler-assessed cerebral blood flow velocity in the neonate as estimator of global cerebral blood volume flow measured using phase-contrast magnetic resonance angiography. Neonatol 2013;103:21–6.
39. Jain V, Buckley EM, Licht DJ, et al. Cerebral oxygen metabolism in neonates with congenital heart disease quantified by MRI and optics. J Cereb Blood Flow Metab 2014;34:380–8.
40. Wintermark P, Hansen A, Warfield SK, Dukhovny D, Soul JS. Near-infrared spectroscopy versus magnetic resonance imaging to study brain perfusion in newborns with hypoxic-ischemic encephalopathy treated with hypothermia. Neuroimage 2014;85 Pt 1:287–93.
41. Massaro AN, Bouyssi-Kobar M, Chang T, Vezina LG, du Plessis AJ, Limperopoulos C. Brain perfusion in encephalopathic newborns after therapeutic hypothermia. AJNR Am J Neuroradiol 2013;34:1649–55.
42. Benders MJ, Hendrikse J, De Vries LS, Van Bel F, Groenendaal F. Phase-contrast magnetic resonance angiography measurements of global cerebral blood flow in the neonate. Pediatr Res 2011;69:544–7.
43. Varela M, Groves AM, Arichi T, Hajnal JV. Mean cerebral blood flow measurements using phase contrast MRI in the first year of life. NMR Biomed 2012;25:1063–72.
44. De Vis JB, Petersen ET, de Vries LS, et al. Regional changes in brain perfusion during brain maturation measured non-invasively with Arterial Spin Labeling MRI in neonates. Eur J Radiol 2013;82:538–43.
45. Miranda MJ, Olofsson K, Sidaros K. Noninvasive measurements of regional cerebral perfusion in preterm and term neonates by magnetic resonance arterial spin labeling. Pediatr Res 2006;60:359–63.
46. Chiron C, Raynaud C, Mazière B, et al. Changes in regional cerebral blood flow during brain maturation in children and adolescents. J Nucl Med 1992;33:696–703.
47. Pryds O, Greisen G. Effect of PaCO2 and haemoglobin concentration on day to day variation of CBF in preterm neonates. Acta Paediatr Scand Suppl 1989;360:33–6.
48. Skov L, Pryds O, Greisen G, Lou H. Estimation of cerebral venous saturation in newborn infants by near infrared spectroscopy. Pediatr Res 1993;33:52–5.
49. Altman DI, Perlman JM, Volpe JJ, Powers WJ. Cerebral oxygen metabolism in newborns. Pediatr 1993;92:99–104.
50. Yoxall CW, Weindling AM. Measurement of cerebral oxygen consumption in the human neonate using near infrared spectroscopy: cerebral oxygen consumption increases with advancing gestational age. Pediatr Res 1998;44:283–90.
51. Tyszczuk L, Meek J, Elwell C, Wyatt JS. Cerebral blood flow is independent of mean arterial blood pressure in preterm infants undergoing intensive care. Pediatr 1998;102(2 Pt 1):337–41.
52. Liu P, Huang H, Rollins N, et al. Quantitative assessment of global cerebral metabolic rate of oxygen (CMRO2) in neonates using MRI. NMR Biomed 2014;27:332–40.
53. Zaramella P, Saraceni E, Freato F, et al. Can tissue oxygenation index (TOI) and cotside neurophysiological variables predict outcome in depressed/asphyxiated newborn infants? Early Hum Dev 2007;83:483–9.
54. van der Aa NE, Porsius ED, Hendrikse J, et al. Changes in carotid blood flow after unilateral perinatal arterial ischemic stroke. Pediatr Res 2012;72:50–6.
55. Wintermark P, Warfield SK. New insights in perinatal arterial ischemic stroke by assessing brain perfusion. Transl Stroke Res 2012;3:255–62.
56. De Vis JB, Petersen ET, Kersbergen KJ, et al. Evaluation of perinatal arterial ischemic stroke using noninvasive arterial spin labeling perfusion MRI. Pediatr Res 2013;74:307–13.
57. Lim CC, Petersen ET, Ng I, Hwang PY, Hui F, Golay X. MR regional perfusion imaging: visualizing functional collateral circulation. AJNR Am J Neuroradiol 2007;28:447–8.
58. Viallon M, Altrichter S, Pereira VM, et al. Combined use of pulsed arterial spin-labeling and susceptibility-weighted imaging in stroke at 3T. Eur Neurol 2010;64:286–96.
59. Yamashita E, Kanasaki Y, Fujii S, Tanaka T, Hirata Y, Ogawa T. Comparison of increased venous contrast in ischemic stroke using phase-sensitive MR imaging with perfusion changes on flow-sensitive alternating inversion recovery at 3 Tesla. Acta Radiol 2011;52:905–10.
60. De Vis JB, Hendrikse J, Petersen ET, et al. Arterial spin-labelling perfusion MRI and outcome in neonates with hypoxic-ischemic encephalopathy. Eur Radiol 2015;25:113–21.
61. Shi H, Song D, Zhang YX, et al. [Analysis of arterial spin labeling in 33 patients with hypoxic ischemic encephalopathy]. Zhonghua Er Ke Za Zhi 2012;50:131–5.

62. Pienaar R, Paldino MJ, Madan N, et al. A quantitative method for correlating observations of decreased apparent diffusion coefficient with elevated cerebral blood perfusion in newborns presenting cerebral ischemic insults. Neuroimage 2012;63:1510–8.
63. Wintermark P, Moessinger AC, Gudinchet F, Meuli R. Temporal evolution of MR perfusion in neonatal hypoxic-ischemic encephalopathy. J Magn Reson Imaging 2008;27:1229–34.
64. Roth SC, Baudin J, Cady E, et al. Relation of deranged neonatal cerebral oxidative metabolism with neurodevelopmental outcome and head circumference at 4 years. Dev Med Child Neurol 1997;39:718–25.
65. Goff DA, Buckley EM, Durduran T, Wang J, Licht DJ. Noninvasive cerebral perfusion imaging in high-risk neonates. Semin Perinatol 2010;34:46–56.
66. Wang J, Licht DJ, Silvestre DW, Detre JA. Why perfusion in neonates with congenital heart defects is negative–technical issues related to pulsed arterial spin labeling. Magn Reson Imaging 2006;24:249–54.
67. Licht DJ, Wang J, Silvestre DW, et al. Preoperative cerebral blood flow is diminished in neonates with severe congenital heart defects. J Thorac Cardiovasc Surg 2004;128:841–9.
68. Nagaraj UD, Evangelou IE, Donofrio MT, et al. Impaired global and regional cerebral perfusion in newborns with complex congenital heart disease. J Pediatr 2015;167:1018–24.
69. Bolar DS, Rosen BR, Sorensen AG, Adalsteinsson E. QUantitative Imaging of eXtraction of oxygen and TIssue consumption (QUIXOTIC) using venular-targeted velocity-selective spin labeling. Magn Reson Med 2011;66:1550–62.